# Methanol to Olefin Conversion on HSAPO-34 Zeolite from Periodic Density Functional Theory Calculations: A Complete Cycle of Side Chain Hydrocarbon Pool Mechanism

**Chuan-Ming Wang,[†,‡] Yang-Dong Wang,[†] Zai-Ku Xie,*[,†] and Zhi-Pan Liu*[,‡]**

*Shanghai Research Institute of Petrochemical Technology, SINOPEC, Shanghai 201208, China, and Department of Chemistry, Fudan University, Shanghai 200433, China*

*Received: November 25, 2008; Revised Manuscript Received: January 21, 2009*

For its unique position in the coal chemical industry, the methanol to olefin (MTO) reaction has been a hot topic in zeolite catalysis. Due to the complexities of catalyst structure and reaction networks, many questions such as how the olefin chain is built from methanol remain elusive. On the basis of periodic density functional theory calculations, this work establishes the first complete catalytic cycle for MTO reaction via hexamethylbenzene (HMB) trapped in HSAPO-34 zeolite based on the so-called side chain hydrocarbon pool mechanism. The cycle starts from the methylation of HMB that leads to heptamethylbenzenium ion (heptaMB$^+$) intermediate. This is then followed by the growth of side chain via repeated deprotonation of benzenium ions and methylation of the exocyclic double bond. Ethene and propene can finally be released from the side ethyl and isopropyl groups of benzenium ions by deprotonation and subsequent protonation steps. We demonstrate that (i) HMB/HSAPO-34 only yields propene as the primary product based on the side chain hydrocarbon pool mechanism and (ii) an indirect proton-shift step mediated by water that is always available in the system is energetically more favorable than the traditionally regarded internal hydrogen-shift step. Finally, the implications of our results toward understanding the effect of acidity of zeolite on MTO activity are also discussed.

## 1. Introduction

As a promising alternative for the synthesis of light olefins, the catalytic conversion of methanol to olefin (MTO) on zeolite catalysts has attracted much recent attention in both industrial and academic communities.[1−12] It was shown that zeolites such as HSAPO-34 and ZSM-5 can efficiently catalyze MTO with high selectivity toward ethene and propene, and the amounts of ethene and propene in the product are generally comparable.[2−4,12−14] Despite the huge efforts devoted to elucidating the carbon−carbon bond formation mechanism from methanol, the central step in the MTO reaction,[1,2,15−17] some important issues are still poorly understood due to the complexities of both the catalyst structure and the reaction itself. A better atomic-level understanding on the zeolite-catalyzed MTO reaction is therefore urgently required.

As for the mechanism of olefin production, a number of possible reaction intermediates have been suggested in the literature.[2] Most naturally, it was long believed that the C−C chain is built by the direct coupling of C1 species, including carbenium ($CH_3^+$), carbene ($:CH_2$), methyl radical ($^{\bullet}CH_3$), or even oxoniumylide ($R_1R_2O^+CH_2^+$). But nowadays these direct mechanisms are out of favor because of the high energy barriers needed for the formation of the C−C bond.[1,2,18−21] Theoretically, Lesthaeghe calculated the oxoniumylide mechanism based on a pentatetrahedral (5T) cluster model, which showed that the ylides are highly unstable and the barriers are very high for the C−C bond formation.[19,20] As an alternative, an indirect hydrocarbon pool mechanism has gleaned more and more experimental and theoretical support,[22−52] in which olefins were suggested to be obtained by the elimination from the side chain of methylated organic intermediates trapped in zeolites. In particular, polymethylbenzenes encapsulated in zeolites identified in the MTO reaction were proposed as the active organic centers.[25,26]

As for the catalytic role of organic active centers, it is suggested to be the species from which the alkyl side chain can be formed or be eliminated into olefins.[22] This suggested mechanism is known as the side chain pathway, which have been proved to be the predominant route for the MTO reaction on zeolites.[31] Theoretically, Haw et al. studied the thermodynamic aspects of the side chain pathway based on simplified cluster models using polymethylbenzenes as the active species, including *p*-xylene, tetramethylbenzene, and hexamethylbenzene.[49] It was indicated that the organic intermediates with an exocyclic double bond are relatively unstable. More recently, the role of zeolite topology for the *gem*-methylation step involved in the side chain pathway on three different zeolites (BEA, CHA, and MFI) was investigated with QM/MM methods.[46] It was shown that the cage of CHA can better stabilize the heptamethylbenzenium ion than the other two cages, which was proposed as the key intermediate for the MTO reaction.

Despite the great progress made in recent years, some key issues in the field remain unclear. In particular, it is not known whether the two main products, ethene and propene, follow a similar reaction pathway or one of them is in fact produced later in the sequence, e.g., from a secondary process.[37−39] In addition, the key factors affecting the zeolite catalytic activity, such as the acidity of the zeolite and the effect of cofeed such as water, have been hotly studied to optimize the activity and selectivity.[53,54] The physical origin of their effects is however not clear as the detailed kinetic information on the rate-determining step is required. State-of-the-art theoretical simulation can be an ideal approach to explore this complex catalytic conversion. To reduce the computational load, zeolites were

* Corresponding author. E-mail: xiezk@sript.com.cn and zpliu@fudan.edu.cn.
† Shanghai Research Institute of Petrochemical Technology.
‡ Fudan University.

10.1021/jp810350x CCC: $40.75 
Published on Web 02/23/2009

traditionally modeled by finite cluster and more recently by QM/MM methods, which suffers from the limitation of accuracy in treating the zeolite framework effect. As an alternative, the first-principle periodic calculations can be a better choice as both the short- and long-range interactions between zeolite framework and reaction center can be taken into account.[49] Therefore, a full exploration of the mechanism of the MTO reaction by the first-principle periodic calculations is timely required for the design of better catalysts for the MTO reaction.

In this work, we utilize periodic density functional theory calculations to verify the side chain hydrocarbon pool mechanism of the MTO reaction via hexamethylbenzene intermediate over HSAPO-34 zeolite. We focus on the following two key questions on reaction kinetics: (i) Can a complete catalytic cycle via the side chain mechanism indeed be established and, if yes, what is the selectivity to ethene and to propene in this mechanism, and (ii) what is the rate-determining step and how would this step be affected by the acidity of zeolite? This paper will be organized as follows. In Section 2, the calculation details and the modeling will be briefly summarized. Our results for the whole reaction map will be addressed in Section 3. This will be followed by discussions in Section 4 on the activity and selectivity in the context of experimental findings. The conclusions are drawn in Section 5.

## 2. Computational Methods and Modeling

All density functional theory (DFT) calculations were performed with the DMol3 package with the double numerical polarization (DNP) basis set and the generalized gradient corrected Perdew−Burke−Ernzerhof (GGA-PBE) functional.[55−57] The real space cutoff distance was 5.0 Å. The core electrons of all atoms were represented by semicore pseudopotentials (DSPP).[58] The reciprocal-space integration over the Brillouin zone was approximated by summing over a finite set of *k*-points with a grid separation of 0.05 $Å^{-1}$ according to the Monkhorst−Pack scheme.[59] The convergence criteria for energy, force, and displacement were $1 \times 10^{-4}$ hartree, $4 \times 10^{-3}$ hartree/Å, and $5 \times 10^{-3}$ Å, respectively. To determine the reaction barrier of reactions, the method combing the linear synchronous transition (LST) and the quadratic synchronous transition (QST) search was employed, which was followed finally by transition state optimization through the eigenvector following method based on vibrational analysis.[60,61] The calculated reaction energies of $2CH_3OH \rightarrow C_2H_4 + 2H_2O$ and $3CH_3OH \rightarrow C_3H_6 + 3H_2O$ are 0.03 and −0.60 eV, respectively, which are consistent with the previous calculated results.[49]

Acid silicoaluminophosphate HSAPO-34 catalyst has a chabazite-related (CHA) structure with cages 1 nm in dimension and a small channel of 0.38 nm.[2,62−64] Our optimized HSAPO-34 cell ($a = b = c = 9.421$ Å, $\alpha = \beta = \gamma = 94.2°$) is depicted in Figure 1a, which was modeled through the substitution of all Si atoms in the CHA framework by P and Al atoms alternatively, and then one P atom replaced by an Si atom. This model contains one Brønsted acid site per cage. In our simulation of reactions, all atoms in the supercell are allowed to relax with the lattice constants of the supercell being fixed.

## 3. Results

The organic active center used in our modeling is hexamethylbenzene (HMB) and the optimized structure of it in HSAPO-34 is shown in Figure 1b. As shown, HMB lies inside the cages of HSAPO-34 with a quasiplaner structure. The shortest distance between HMB and the framework of zeolite is 2.5 Å, which is the distance between the H atom in the methyl group and a framework O atom. In this structure, the HMB cannot rotate easily inside the cage due to the steric effect.

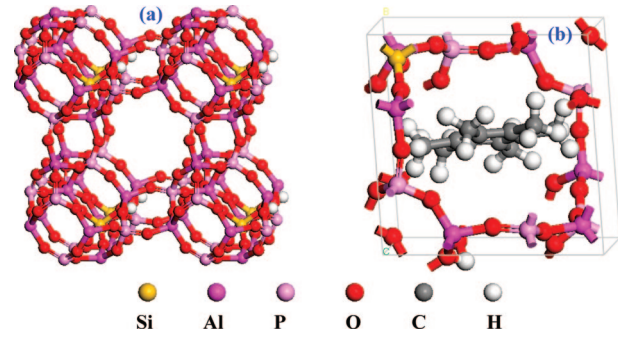


**Figure 1.** Structures of HSAPO-34 zeolite (a) and hexamethylbenzene in HSAPO-34 (b). The shape of the cage and composited rings of HSAPO-34 are highlighted in part a.

As proposed by experiment, HMB can act as the center for the growth of the C−C chain following the so-called side chain hydrocarbon pool mechanism. We have explored this mechanism thoroughly by locating all the likely transition states of the elementary steps. Our determined pathway is summarized in Scheme 1 and the corresponding energy profile is shown in Figure 2. As shown, this side chain pathway involves the propagation of side chain by the methylation step, that is M4 → M5 and M9 → M10, and the elimination of side chain by the internal H-shift or indirect proton-shift step, which includes steps M5 → M7 and M10 → M12. The pathway leading to propene differs from that leading to ethene at the stage of M5, where the former continues the chain growth by M5 → M8 while the latter undergoes H-shift to M7.

Among the intermediates, the benzenium ions M2, M5, and M10 were believed to be the key intermediates. Arstad et al. suggested that olefins are eliminated from the side chain by the internal H-shift step.[49] However, we found that the internal 1,3-H-shift step is highly kinetically hindered while a two-step deprotonation/protonation with the participation of zeolite acid site is much lower in the reaction barrier. In this two-step indirect pathway, our calculations identified two new intermediates M6 and M11, which feature the spiro structure composed of a three-membered carbon ring and a six-membered carbon ring. They are in fact the most unstable intermediates leading to the production of ethene and propene, respectively, and they thus determine largely the barrier height of olefin formation.

In the following, we will go through our results in detail by focusing on the energetics and the structures of each elementary step as those reported in Scheme 1 and Figure 2.

**3.1. M1 → M5: Formation of Ethyl Group in the Side Chain.** The capture of methanol by the acid site of zeolite is the first step to initiate the MTO reaction. The adsorption energy of methanol in HSAPO-34 zeolite is calculated to be 0.90 eV and the adsorption structure is shown in Figure 3 (M1). There are two obvious H-bondings for methanol interacting with the zeolite framework. The first one involves the solid-acid proton from zeolite interacting with the hydroxyl O of methanol. This interaction is strong, as reflected by the extremely short ZOH···OHMe distance, 1.23 Å, indicating that the methanol near the acid site can be considered as a protonated methanol $CH_3OH_2^+$. This may explain why the calculated adsorption energy of methanol is large, being much stronger than that typical H-bonding can afford. The second hydrogen bonding is rather typical, through ZO···HOMe linkage with a distance of 1.89 Å. Our optimized structure of methanol on HSAPO-34 is similar to that of methanol on CHA.[65]

**SCHEME 1: Catalytic Cycle of the Side Chain Hydrocarbon Pool Mechanism for the MTO Reaction[a]**

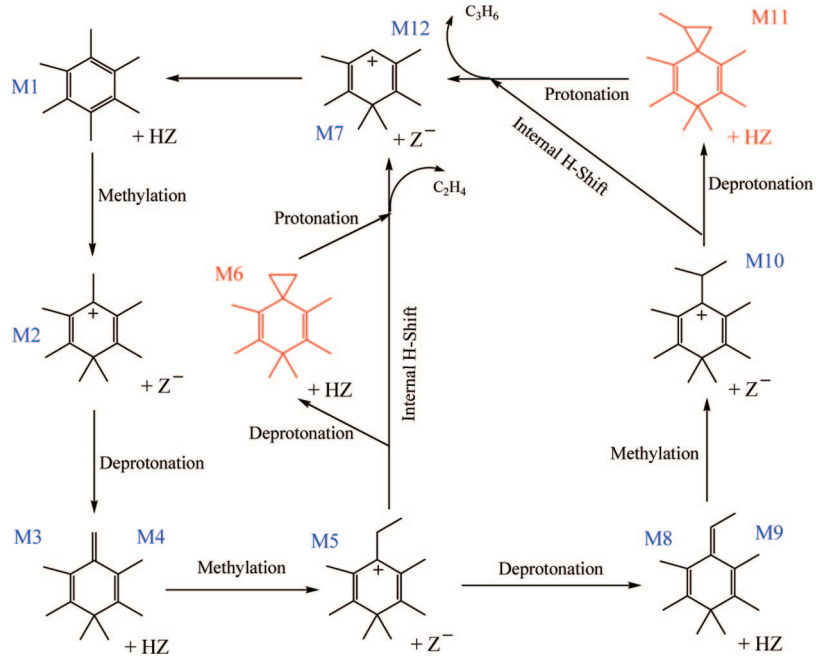


[a] The zeolite is abbreviated by HZ. M3 and M4 refer to the same organic intermediate but with different coadsorption species, one with water and another with methanol. The same is true for M8 and M9.

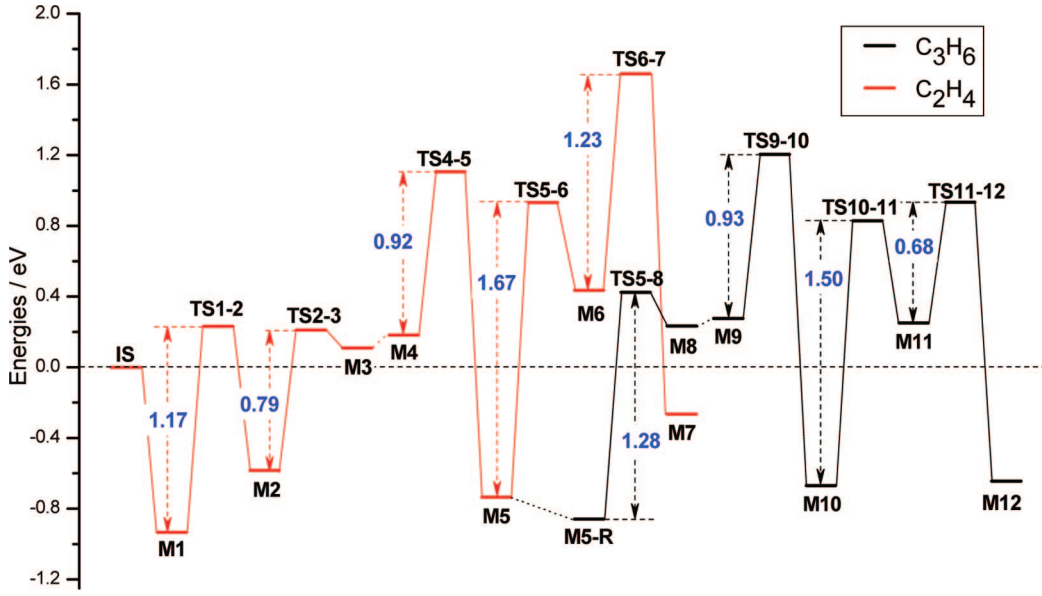


**Figure 2.** Energy profile of the side chain hydrocarbon pool mechanism for MTO reaction on the HMB/HSAPO-34 model (also see Scheme 1 for the structure of each state). All energies are referenced to the energy of HMB/HSAPO-34 and three methanol molecules in the gas phase (IS).

In the presence of HMB species inside the cage of zeolite, the adsorbed methanol can attack HMB species through a $S_N2$-type transition state (TS1-2). After the TS, the heptamethylbenzenium ion (heptaMB$^+$) and the water molecule are produced. The involved initial (M1), transition state, and intermediate (M2) structures are shown in Figure 3. This methylation step needs to overcome an energy barrier of 1.17 eV, and is endothermic by 0.35 eV. At TS1-2, the central methyl group adopts a quasiplanar structure. The breaking O−C bond is 2.20 Å and the forming C−C bond is 2.23 Å with the O−C−C angle being about 173° (geometry close to linearity). Such structural features are typical for $S_N2$-type reactions.

The formed heptaMB$^+$ can lose its proton from the side chain methyl group to the framework of HSAPO-34, which yields the intermediate HMMC (M3) as shown in Figure 3. We found that there are two possible pathways of deprotonation for heptaMB$^+$. In the first scenario (see Figure 3 (TS2-3-D)), heptaMB$^+$ loses its proton to the zeolite framework directly. The calculated energy barrier equals 1.28 eV, and the reaction is endothermic by 1.24 eV. This indicates that the intermediate HMMC is unstable and can decay back to heptaMB$^+$ easily. However, if a water molecule is added into the cage, the proton passing between organic species and zeolite framework can be significantly facilitated. The calculated reaction barrier from M2

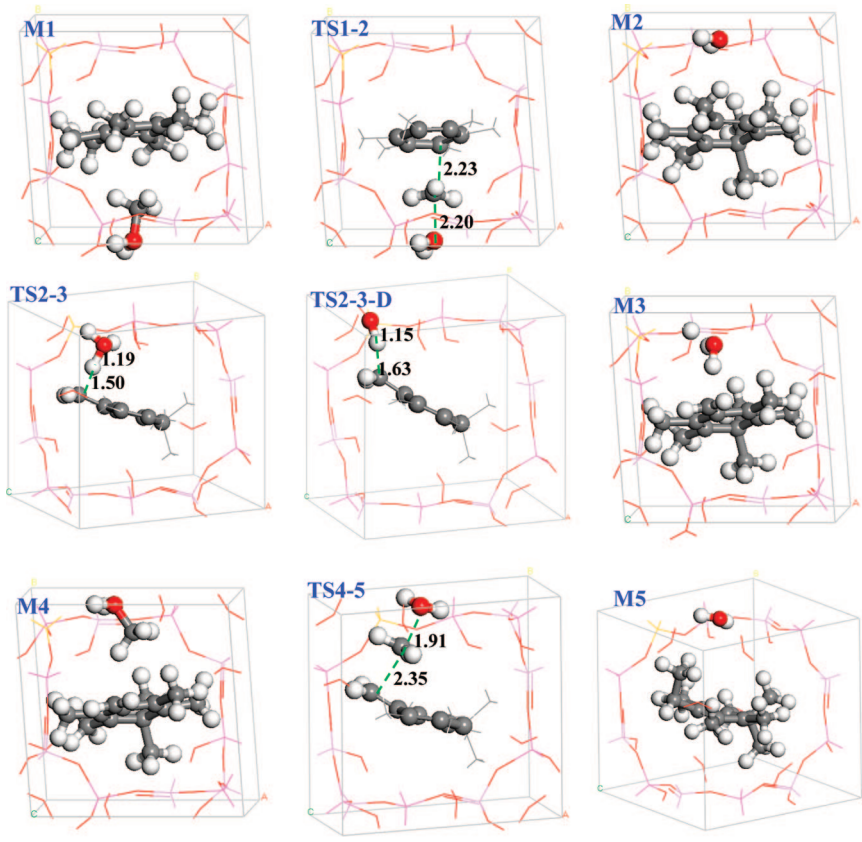


**Figure 3.** Initial, transition state, and intermediate structures for the formation of M5. The unit of labeled interatomic distances is Å.

to M3 decreases to 0.80 eV, and the reaction is only endothermic by 0.69 eV. The energy of M3 is about 1.04 eV higher than that of M1. The TS (TS2-3 in Figure 3) is final-state-like with a much-lengthened C−H distance of 1.50 Å but a much shorter H−$OH_2$ distance of 1.19 Å.

It is evident that water can function as a bridge between organic species and the zeolite framework. It decreases significantly the barrier of proton shift. This may be understood as water can better stabilize the final state than the initial state. The change in endothermicity of the reaction helps to reduce the reaction barrier. From our calculations, it can be seen that at the final state the ZOH···$OH_2$ distance is as short as 1.35 Å, consistent with the large adsorption energy (0.92 eV) of $H_2O$ at the intermediate M3.

The next step is the methylation of HMMC, which involves a second methanol to attack the exocyclic double bond of HMMC to form a side ethyl group. The formed intermediate is 1,1,2,3,5,6-hexamethyl-4-ethylbenzenium ion (M5). The step needs to overcome an energy barrier of 0.92 eV, and is exothermic by 0.92 eV. The energy of M5 is about 0.20 eV higher than that of M1. By comparing with the first methylation step from M1 to M2, we can see that the methylation of the exocyclic double bond is slightly easier than that of the ring carbons of HMB. The structural features of the transition state TS4-5 are similar to those of TS1-2 except that the breaking/forming bond distances (O−C: 1.91 Å; C−C: 2.35 Å) are slightly varied. It should be mentioned that the propagation of the side chain as achieved in this methylation step is not the most difficult kinetic step and thus should not be the rate-determining step for olefin formation. Starting from the common intermediate M5, the routes leading to ethene and propene bifurcate and they will be elaborated individually.

**3.2. M5 → M7: Production of Ethene.** To produce ethene, one ending H of the side ethyl group has to be shifted to the ring carbon. The reaction is traditionally regarded to occur through a direct internal H-shift step. Our calculated results, however, indicate that the barrier of this internal H-shift step is as high as 2.89 eV. At the transition state (TS-D-C2H4 in Figure 4), the breaking C−H in the $CH_3$ group is much elongated to 1.80 Å, while the C−C interatomic distance between the ethyl and ring carbon is 1.70 Å.

In parallel to the direct mechanism, an indirect pathway of H-passing is in fact energetically more likely, which involves M5 first deprotonation to the zeolite, M5 → M6, and the return of the proton to the ring carbon from the zeolite, M6 → M7. Both steps are mediated by a nearby $H_2O$. The corresponding intermediate (M6), transition state structures (TS5-6, TS6-7) for the elimination of ethene are shown in Figure 4. As can be seen from Figure 2, the reaction barriers for the deprotonation and protonation steps are 1.67 and 1.23 eV, respectively. Because the barrier of M6 back to M5 is only 0.50 eV, much lower than that of M6 to M7, it is conceived that the production of ethene needs to overcome an overall 2.40 eV energy barrier from M5 to M7, which is 0.49 eV lower than the direct H-shift mechanism.

The organic intermediate M6 features a side spiro structure with the angles of the three-membered ring being 58.5°, 61.4°, and 60.1°, respectively. Because of the imposed strain of the small ring, M6 is relatively unstable, and the energy of M6 is about 1.36 eV higher than that of M1. For the structure of transition state TS5-6, the distances of C3−H in the $CH_3$ group and C3−C1 are 1.44 and 1.74 Å, respectively. At the TS6-7, the two key C−C distances, C2C1 and C3C1, are lengthened to 2.28 and 1.74 Å, respectively.

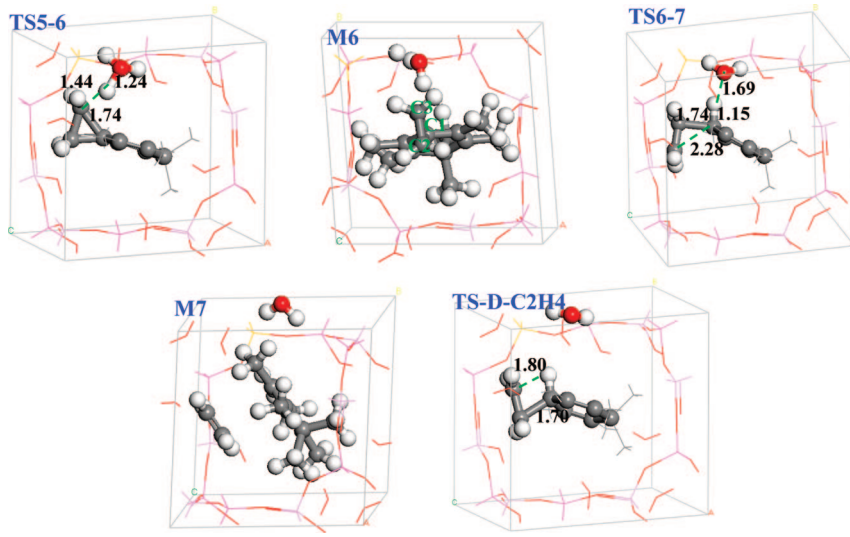


**Figure 4.** Intermediate and transition state structures for the production of ethene. The unit of labeled interatomic distances is Å.

It is of interest to ask why the indirect proton-shift step for the elimination of ethene is energetically more feasible than the internal H-shift. From the structural features, we found that this may be attributed to the structural distortion energy cost at the transition state. In Figure 4, we showed that the bond angle C3C2C1 at TS-D-C2H4 is 71.2°, while the bond angle C2C3C1 is 92.7° at TS6-7. The former has a larger deviation from standard $sp^3$ hybridization angle. It is conceivable that the strain at the side chain of TS-D-C2H4 results in the high energy barrier for the elimination of ethene via the internal H-shift step.

**3.3. M5 → M12: Production of Propene.** Different from the route to ethene, propene is produced via the deprotonation of the $CH_2$ of the side ethyl group in M5, as shown in Figure 5. The intermediate 1,2,3,3,4,5,-hexamethyl-6-ethylidene-1,4-cyclohexadiene (HMEC) with an exocyclic double bond is formed (M5-R → M8). This step requires an energy barrier of 1.29 eV and is endothermic by 1.09 eV. The energy of M8 is about 1.16 eV higher than that of M1. The side chain can then propagate (M9 to M10) through the methylation of the exocyclic double bond in HMEC by a third adsorbed methanol molecule. For the methylation step, the transition state structure (TS9-10) and the reaction barrier (0.93 eV) bear great similarity with those in previous methylation steps (M4 → M5), as shown in Figure 5.

Similar to those found in the ethene production route, the production of propene also prefers the indirect proton-shift pathway. The direct pathway of the H-shift from M10 to M12 is hindered by a reaction barrier of 2.05 eV and the transition state structure is as shown in Figure 5 (TS-D-C3H6). By contrast, the indirect pathway involves the deprotonation of M10 to M11 and the protonation of M11 that leads to the elimination of propene. The former reaction needs to overcome an energy barrier of 1.50 eV, and is endothermic by 0.92 eV, while the latter reaction is relatively facile with the barrier of 0.68 eV. Overall, the barrier from M10 to propene is 1.60 eV in the indirect pathway, being 0.45 eV more favorable than the direct internal H-passing pathway. It is noticed that the geometry structure of M11 is very similar to that in M6, featuring a side spiro structure. The energy of M11 is about 1.18 eV higher than that of M1.

By comparing the step of M6 → M7 in the ethene production pathway and M11 → M12 in the propene production pathway, we can see that the barrier to propene (0.68 eV) is much less than that to ethene (1.23 eV). This can be attributed to the stability of the transition state structure where a hydrocarbon cation is forming through the protonation at the side chain $\beta$-C. For the propene formation (TS11-12) the $\beta$-C is a secondary carbon, while that in the ethene formation (TS6-7) is a primary carbon. Therefore, it is not surprising that TS11-12 is energetically more stable than TS6-7.

**3.4. Regeneration of Hexamethylbenzene.** The elimination of ethene and propene from M5 and M10 leaves the 1,1,2,3,5,6-hexamethylbenzenium ion in the HSAPO-34 cage. The hexamethylbenzene can be regenerated by methyl shifts and proton shift in order to complete the catalytic cycle. Our calculated energy profile and some represented transition state structures are shown in Figure 6. The energy barriers for the shifts of methyl on the carbon ring are in the range of 0.79−0.91 eV, which is consistent with the previous calculation where the 1,2-methyl shift activation energy was calculated to be 0.90 eV for the gas phase heptaMB$^+$.[48] The formed 1,2,3,4,5,6-hexamethylbenzenium ion can finally lose a proton from its benene ring to regenerate HMB. The energy barrier of this step is only 0.12 eV. Since all these reaction barriers are generally lower than those required for olefin formation, it can be concluded that organic reaction center HMB in the cage of the HSAPO-34 zeolite can easily be regenerated at reaction conditions.

## 4. General Discussions

The side chain hydrocarbon pool mechanism explored here by periodic DFT calculations indicated that the intermediates with an exocyclic double bond are relatively unstable species among all the intermediates except the new proposed spiro intermediates M6 and M11. This is consistent with the calculated results for the stability of intermediates in the gas phase.[49] As can be seen from the periodic DFT calculated results, the methylation energy barrier of HMB in HSAPO-34 zeolite is 1.17 eV. It should be mentioned that the energy barrier of this HMB *gem*-methylation step on CHA zeolite is 0.63 eV by QM/MM methods.[46] This energy barrier difference may be related to the composition and modeling of zeolite.

As can be seen from Figure 2, the rate-determining step for the production of ethene is the protonation of organic intermediate M6, while that for the production of propene is the methylation of an exocyclic double bond in M9. It was

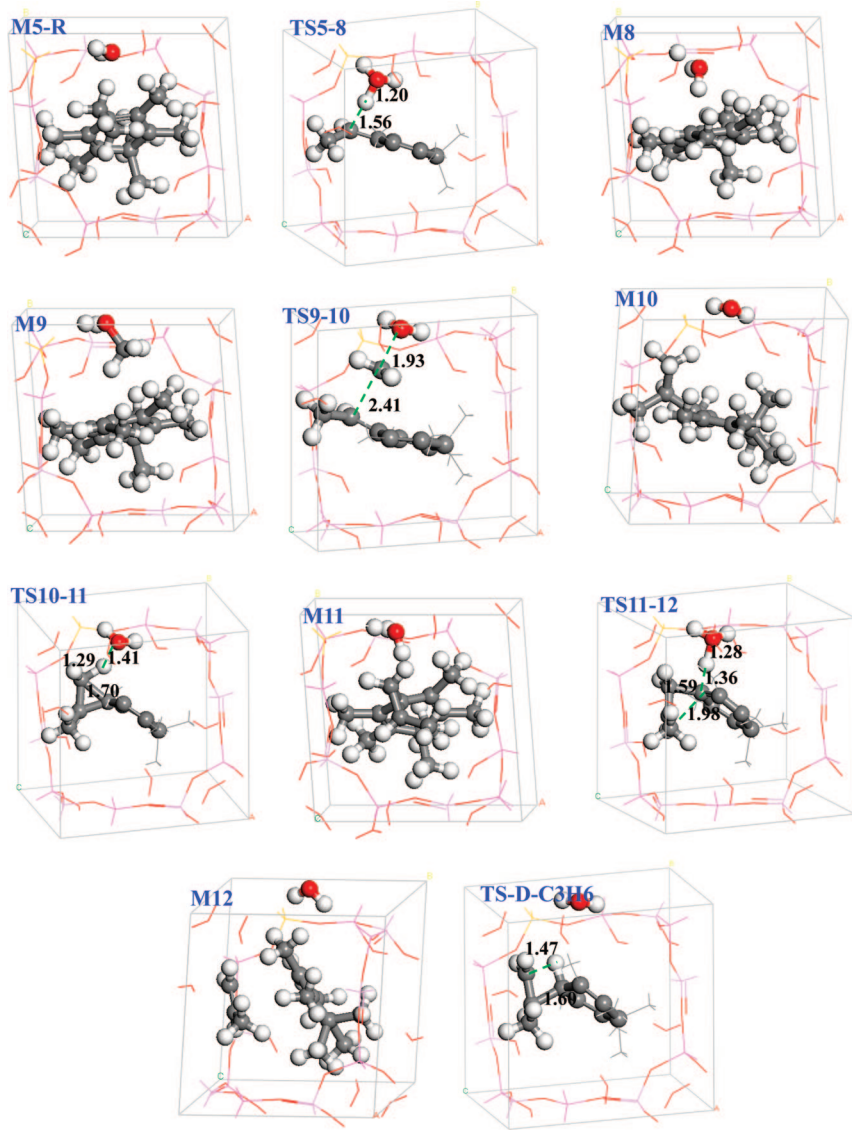


**Figure 5.** Intermediate and transition state structures for the production of propene. The unit of labeled interatomic distances is Å.

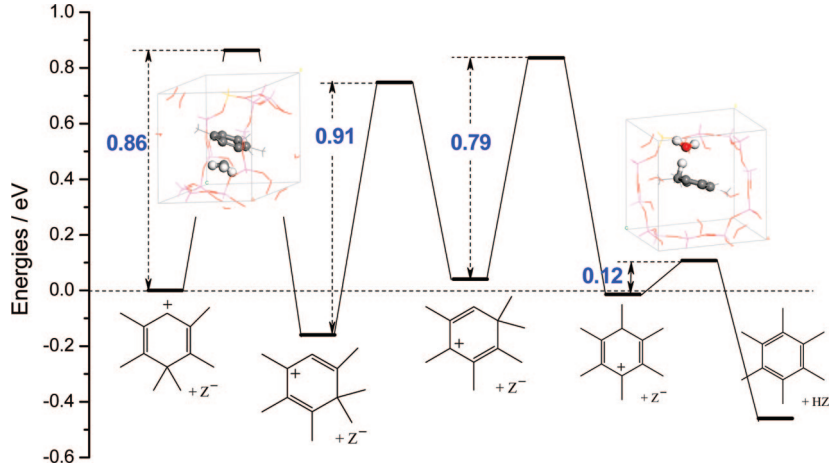


**Figure 6.** Energy profile and representative transition state structures for the regeneration of HMB in HSAPO-34 zeolite.

calculated that the overall energy barrier of the rate-determining step for the production of ethene is 2.40 eV (from M5 to M7), and that for the production of propene is 2.14 eV (from M5-R to M10). The propene is therefore a preferential olefin product through the side chain hydrocarbon pool mechanism for the MTO reaction catalyzed by HMB in the HSAPO-34 zeolite. Furthermore, both rate-determining steps are related to the ability of zeolite to donate protons. It can thus be concluded that the

activity of the MTO reaction by HMB/HSAPO-34 can be improved by the increase of acidity of the HSAPO-34 zeolite considering that the energy barriers of protonation and methylation of organic species should be reduced by the increase of zeolite acidity.

Another important feature from our calculations is that water has to take part in the indirect proton-shift reaction for the elimination of olefins. It is difficult for a proton to shift directly from zeolite framework to the carbon ring (M6 → M7 and M11 → M12) in the absence of water. This can be attributed to the structural feature of the zeolite cage. First, the distance between the shifted proton in the zeolite framework and the ring carbon of organic intermediates is quite long (about 4 Å). Second, the rotation of the organic intermediates in the pore of zeolite is also hindered by the steric effect. Our results are consistent with the experimental findings that the addition of water to the feed with methanol can help to maximize the selectivity to olefins over the HSAPO-34 zeolite.[53,54] It should also be noticed that one of the main products of the MTO reaction is water and the promoting role of water with feed becomes indistinguishable as the reaction continues.

## 5. Conclusions

The side chain hydrocarbon pool mechanism for the MTO reaction by hexamethylbenzene encapsulated in HSAPO-34 zeolite was thoroughly investigated by the periodic density functional theory method. Two new intermediates are identified for the elimination of ethene and propene in order to overcome the high energy barriers in the internal H-shift steps. These two intermediates feature the side chain spiro structure, and are very unstable compared to the benzenium ion in the HSAPO-34 zeolite. Our results indicate that HMB/HSAPO-34 selectively produce propene, not ethene. It is shown that the MTO activity of HMB/HSAPO-34 is largely determined by the efficiency of the protonation of organic intermediates and the methylation of exocyclic double bonds involved in the side chain route. Both steps are related to the acidity of zeolite. The promoting role of water is also identified. Water can act as the bridging species to facilitate the proton shift between organic species and the zeolite framework and also as a hydrogen-bonding acceptor to stabilize the solid acid.

**Acknowledgment.** This work is supported by National Basic Research Program of China (2009CB623504), National Science Foundation of China (20773026, 20721063, J0730419), and China Postdoctoral Science Foundation (20080440568).

## References and Notes

(1) Stocker, M. *Microporous Mesoporous Mater.* **1999**, *29*, 3.
(2) Haw, J. F.; Song, W. G.; Marcus, D. M.; Nicholas, J. B. *Acc. Chem. Res.* **2003**, *36*, 317.
(3) Haw, J. F.; Marcus, D. M. *Top. Catal.* **2005**, *34*, 41.
(4) Chen, J. Q.; Bozzano, A.; Glover, B.; Fuglerud, T.; Kvisle, S. *Catal. Today* **2005**, *106*, 103.
(5) Bhan, A.; Iglesia, E. *Acc. Chem. Res.* **2008**, *41*, 559.
(6) Chen, D.; Rebo, H. P.; Moljord, K.; Holmen, A. *Ind. Eng. Chem. Res.* **1999**, *38*, 4241.
(7) Dahl, I. M.; Mostad, H.; Akporiaye, D.; Wendelbo, R. *Microporous Mesoporous Mater.* **1999**, *29*, 185.
(8) Keil, F. J. *Microporous Mesoporous Mater.* **1999**, *29*, 49.
(9) Mikkelsen, O.; Kolboe, S. *Microporous Mesoporous Mater.* **1999**, *29*, 173.
(10) Djieugoue, M. A.; Prakash, A. M.; Kevan, L. *J. Phys. Chem. B* **2000**, *104*, 6452.
(11) Zhu, Q. J.; Kondo, J. N.; Ohnuma, R.; Kubota, Y.; Yamaguchi, M.; Tatsumi, T. *Microporous Mesoporous Mater.* **2008**, *112*, 153.
(12) Park, J. W.; Lee, J. Y.; Kim, K. S.; Hong, S. B.; Seo, G. *Appl. Catal. A: Gen.* **2008**, *339*, 36.
(13) Liu, G. Y.; Tian, P.; Zhang, Y.; Li, J. Z.; Xu, L.; Meng, S. H.; Liu, Z. M. *Microporous Mesoporous Mater.* **2008**, *114*, 416.
(14) Liu, G. Y.; Tian, P.; Li, J. Z.; Zhang, D. Z.; Zhou, F.; Liu, Z. M. *Microporous Mesoporous Mater.* **2008**, *111*, 143.
(15) Wang, W.; Hunger, M. *Acc. Chem. Res.* **2008**, *41*, 895.
(16) Blaszkowski, S. R.; Van Santen, R. A. *J. Am. Chem. Soc.* **1997**, *119*, 5020.
(17) Tajima, N.; Tsuneda, T.; Toyama, F.; Hirao, K. *J. Am. Chem. Soc.* **1998**, *120*, 8222.
(18) Marcus, D. M.; McLachlan, K. A.; Wildman, M. A.; Ehresmann, J. O.; Kletnieks, P. W.; Haw, J. F. *Angew. Chem., Int. Ed.* **2006**, *45*, 3133.
(19) Lesthaeghe, D.; Van Speybroeck, V.; Marin, G. B.; Waroquier, M. *Angew. Chem., Int. Ed.* **2006**, *45*, 1714.
(20) Lesthaeghe, D.; Van Speybroeck, V.; Marin, G. B.; Waroquier, M. *Chem. Phys. Lett.* **2006**, *417*, 309.
(21) Lesthaeghe, D.; Van Speybroeck, V.; Marin, G. B.; Waroquier, M. *Ind. Eng. Chem. Res.* **2007**, *46*, 8832.
(22) Olsbye, U.; Bjorgen, M.; Svelle, S.; Lillerud, K. P.; Kolboe, S. *Catal. Today* **2005**, *106*, 108.
(23) Dahl, I. M.; Kolboe, S. *J. Catal.* **1996**, *161*, 304.
(24) Haw, J. F.; Nicholas, J. B.; Song, W. G.; Deng, F.; Wang, Z. K.; Xu, T.; Heneghan, C. S. *J. Am. Chem. Soc.* **2000**, *122*, 4763.
(25) Song, W. G.; Haw, J. F.; Nicholas, J. B.; Heneghan, C. S. *J. Am. Chem. Soc.* **2000**, *122*, 10726.
(26) Arstad, B.; Kolboe, S. *J. Am. Chem. Soc.* **2001**, *123*, 8137.
(27) Arstad, B.; Kolboe, S. *Catal. Lett.* **2001**, *71*, 209.
(28) Song, W. G.; Fu, H.; Haw, J. F. *J. Phys. Chem. B* **2001**, *105*, 12839.
(29) Song, W. G.; Fu, H.; Haw, J. F. *J. Am. Chem. Soc.* **2001**, *123*, 4749.
(30) Song, W. G.; Nicholas, J. B.; Haw, J. F. *J. Am. Chem. Soc.* **2001**, *123*, 121.
(31) Sassi, A.; Wildman, M. A.; Ahn, H. J.; Prasad, P.; Nicholas, J. B.; Haw, J. F. *J. Phys. Chem. B* **2002**, *106*, 2294.
(32) Song, W. G.; Marcus, D. M.; Fu, H.; Ehresmann, J. O.; Haw, J. F. *J. Am. Chem. Soc.* **2002**, *124*, 3844.
(33) Song, W. G.; Nicholas, J. B.; Sassi, A.; Haw, J. F. *Catal. Lett.* **2002**, *81*, 49.
(34) Wang, W.; Buchholz, A.; Seiler, M.; Hunger, M. *J. Am. Chem. Soc.* **2003**, *125*, 15260.
(35) Bjorgen, M.; Olsbye, U.; Petersen, D.; Kolboe, S. *J. Catal.* **2004**, *221*, 1.
(36) Bjorgen, M.; Olsbye, U.; Svelle, S.; Kolboe, S. *Catal. Lett.* **2004**, *93*, 37.
(37) Svelle, S.; Joensen, F.; Nerlov, J.; Olsbye, U.; Lillerud, K. P.; Kolboe, S.; Bjorgen, M. *J. Am. Chem. Soc.* **2006**, *128*, 14770.
(38) Svelle, S.; Olsbye, U.; Joensen, F.; Bjorgen, M. *J. Phys. Chem. C* **2007**, *111*, 17981.
(39) Bjorgen, M.; Svelle, S.; Joensen, F.; Nerlov, J.; Kolboe, S.; Bonino, F.; Palumbo, L.; Bordiga, S.; Olsbye, U. *J. Catal.* **2007**, *249*, 195.
(40) Wang, W.; Jiang, Y. J.; Hunger, M. *Catal. Today* **2006**, *113*, 102.
(41) Cui, Z. M.; Liu, Q.; Song, W. G.; Wan, L. J. *Angew. Chem., Int. Ed.* **2006**, *45*, 6512.
(42) Cui, Z. M.; Liu, Q.; Baint, S. W.; Ma, Z.; Song, W. G. *J. Phys. Chem. C* **2008**, *112*, 2685.
(43) Cui, Z. M.; Liu, Q.; Ma, Z.; Bian, S. W.; Song, W. G. *J. Catal.* **2008**, *258*, 83.
(44) Goguen, P. W.; Xu, T.; Barich, D. H.; Skloss, T. W.; Song, W. G.; Wang, Z. K.; Nicholas, J. B.; Haw, J. F. *J. Am. Chem. Soc.* **1998**, *120*, 2650.
(45) Palumbo, L.; Bonino, F.; Beato, P.; Bjorgen, M.; Zecchina, A.; Bordiga, S. *J. Phys. Chem. C* **2008**, *112*, 9710.
(46) Lesthaeghe, D.; De Sterck, B.; Van Speybroeck, V.; Marin, G. B.; Waroquier, M. *Angew. Chem., Int. Ed.* **2007**, *46*, 1311.
(47) McCann, D. M.; Lesthaeghe, D.; Kletnieks, P. W.; Guenther, D. R.; Hayman, M. J.; Van Speybroeck, V.; Waroquier, M.; Haw, J. F. *Angew. Chem., Int. Ed.* **2008**, *47*, 5179.
(48) Arstad, B.; Kolboe, S.; Swang, O. *J. Phys. Chem. A* **2005**, *109*, 8914.
(49) Arstad, B.; Nicholas, J. B.; Haw, J. F. *J. Am. Chem. Soc.* **2004**, *126*, 2991.
(50) Svelle, S.; Kolboe, S.; Olsbye, U.; Swang, O. *J. Phys. Chem. B* **2003**, *107*, 5251.
(51) Arstad, B.; Kolboe, S.; Swang, O. *J. Phys. Chem. B* **2004**, *108*, 2300.
(52) Arstad, B.; Kolboe, S.; Swang, O. *J. Phys. Chem. B* **2002**, *106*, 12722.
(53) Wu, X.; Anthony, R. G. *Appl. Catal. A: Gen.* **2001**, *218*, 241.
(54) Wu, X.; Abraha, M. G.; Anthony, R. G. *Appl. Catal. A: Gen.* **2004**, *260*, 63.
(55) Delley, B. *J. Chem. Phys.* **1990**, *92*, 508.
(56) Delley, B. *J. Chem. Phys.* **2000**, *113*, 7756.
(57) Perdew, J. P.; Burke, K.; Ernzerhof, M. *Phys. Rev. Lett.* **1996**, *77*, 3865.

(58) Delley, B. *Phys. Rev. B* **2002**, *66*, 155125.
(59) Monkhorst, H. J.; Pack, J. D. *Phys. Rev. B* **1976**, *13*, 5188.
(60) Govind, N.; Petersen, M.; Fitzgerald, G.; King-Smith, D.; Andzelm, J. *Comput. Mater. Sci.* **2003**, *28*, 250.
(61) Banerjee, A.; Adams, N.; Simons, J.; Shepard, R. *J. Phys. Chem.* **1985**, *89*, 52.
(62) Lok, B. M.; Messina, C. A.; Patton, R. L.; Gajek, R. T.; Cannan, T. R.; Flanigen, E. M. *J. Am. Chem. Soc.* **1984**, *106*, 6092.
(63) Pastore, H. O.; Coluccia, S.; Marchese, L. *Annu. Rev. Mater. Res.* **2005**, *35*, 351.
(64) Hartmann, M.; Kevan, L. *Chem. Rev.* **1999**, *99*, 635.
(65) Shah, R.; Payne, M. C.; Lee, M. H.; Gale, J. D. *Science* **1996**, *271*, 1395.

JP810350X